SIViP (2012) 6:301–315
DOI 10.1007/s11760-010-0193-5

ORIGINAL PAPER

Iris segmentation using game theory

Kaushik Roy · Prabir Bhattacharya · Ching Y. Suen

Received: 2 November 2009 / Revised: 22 October 2010 / Accepted: 26 October 2010 / Published online: 16 November 2010

Abstract Robust segmentation of an iris image plays an important role in iris recognition. However, the nonlinear deformations, pupil dilations, head rotations, motion blurs, reflections, nonuniform intensities, low image contrast, camera angles and diffusions, and presence of eyelids and eyelashes often hamper the conventional iris/pupil localization methods, which utilize the region-based or the gradient-based boundary-finding information. The novelty of this research effort is that we describe a new iris segmentation scheme using game theory to elicit iris/pupil boundaries from a nonideal iris image. We apply a parallel game-theoretic decision making procedure by modifying Chakraborty and Duncan's algorithm, which integrates (1) the region-based segmentation and gradient-based boundary-finding methods and (2) fuses the complementary strengths of each of these individual methods. This integrated scheme forms a unified approach, which is robust to noise and poor localization, and less affected by weak iris/sclera boundaries. The verification and identification performance of the proposed method are validated using the ICE 2005, the UBIRIS Version 1, WVU Nonideal, and the CASIA Version 3 data sets.

K. Roy (✉) · C. Y. Suen
Centre for Pattern Recognition and Machine Intelligence
(CENPARMI), Concordia University, Montreal,
QC H3G 1M8, Canada
e-mail: kaush_ro@encs.concordia.ca

C. Y. Suen
e-mail: suen@encs.concordia.ca

P. Bhattacharya
Department of Computer Science, College of Engineering,
University of Cincinnati, Cincinnati, OH 45221-0030, USA
e-mail: prabir@encs.concordia.ca

Keywords Biometrics · Iris recognition · Iris segmentation · Game theory · Nash equilibrium · Level set methods

1 Introduction

Iris recognition has been acknowledged as one of the most reliable biometric technologies for identity authentication. Currently, iris recognition plays a very important role in many security-related applications, such as accessing-privileged information, border control, national ID card, rapid processing of passengers in airports, homeless tracking, missing person identification, etc [1–3]. As we can see from Fig. 1, the human iris is an annular portion between the pupil and the white sclera [4,5]. The richness of texture details in iris images, such as freckles, coronas, crypts, furrows, etc., and the stability of iris pattern make it a most consistent biometric trait for person authentication [6–11]. Daugman [1–3,11], Ma et al. [4,5], Boles and Boashash [6], Wildes et al. [7,8] and several other researchers [9–39] proposed different iris recognition algorithms. However, the accurate segmentation, as the first and perhaps the most critical step of iris recognition, still remains a challenging issue particularly in a noncooperative environment. The main task of the segmentation routine is to localize the inner/outer boundary from the iris. Apart from the proper localization of the iris structure, the segmentation scheme should also identify the eyelid and eyelash occlusions and detect the other noisy regions such as reflections. The localization error may result in lower recognition performance due to incorrect encoding of the textural content of the iris. Most existing iris segmentation methods use the gradient information to locate the inner and outer boundaries of the iris [1–9,11–19,21–27,30–37]. However, the low-level boundary methods like

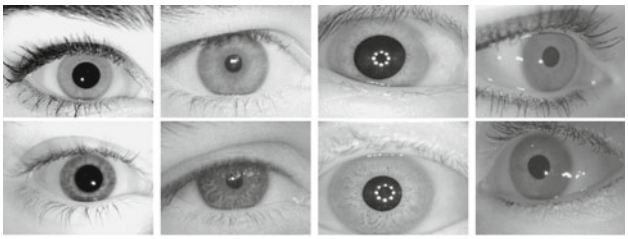

Fig. 1 Sample of iris images. **a** ICE 2005, **b** UBIRIS Version 1, **c** CASIA Version 3, and **d** WVU nonideal data sets

edge detection are not suitable for extracting whole edges as they suffer from false and broken edges. Several researchers applied the deformable whole boundary methods that rely on the gradient features at a subset of the spatial positions of the image [9,11,12,15–17,25–27,35]. This approach handles the discontinuities effectively in the data by imposing the global shape information and is more adaptable to changes in the topology of the object under consideration [40–46]. However, such a method relies on the value of the gradient of the boundary points and thus, suffers from noise sensitivity. Another well-known approach for segmentation is the region-based method that depends on the homogeneity of spatially localized features and other pixel statistics [38,45,46]. The main advantage of these schemes is that they depend directly on the gray-level image and thus, are less susceptible to noise than the other methods that use the derivative information. However, such a region-based scheme suffers from poor localization and over-segmentation. Therefore, the region-based schemes have better noise properties and are less affected by the blurred boundaries, and the boundary-based approaches, on the contrary, have a superior localization performance and work better against the shape variation [45,46]. From the above discussion, it is clear that a better segmentation performance can be achieved if we integrate both the segmentation methods and fuse the complementary strengths of these individual schemes. Recently, several challenges have been identified in the segmentation of iris images that are captured in unconstrained situations. Most state-of-the-art iris recognition algorithms focus on the processing of the ideal iris images that are acquired in a strict imagery setup. However, the segmentation performance is hampered substantially when the iris images are occluded severely by eyelids, eyelashes, shadows, and specular reflections. Moreover, it is observed that, iris boundaries are of arbitrary shapes and therefore can lead to segmentation error if the irises are fitted with the assumption that they always maintain a particular shape. Other factors that degrade the segmentation performance include gaze deviation, defocusing, motion blur, poor contrast, oversaturation, etc [31]. In this research effort, we use the methodologies to account for such disturbances to develop a robust nonideal iris segmentation scheme using game theory which integrates the complementary strengths of the region-based and gradient-based boundary-finding methods.

The rest of this paper is organized as follows. In Sect. 2, we discuss the related work on the state-of-the-art iris segmentation algorithms. Section 3 describes the proposed iris segmentation technique based on game-theoretic approach and also discusses the noise reduction approaches. The experimental results, comparisons with the state-of-the-art algorithms, and discussions are reported in Sect. 4. Section 5 provides our conclusions.

2 Related work

Several researchers proposed different techniques for the segmentation. Daugman [1–3] used the integro-differential operator to segment the iris. Boles and Boashash [6] applied the edge detection method and other image-processing techniques to localize the iris region. Wildes [7] employed the binary edge map and the Hough transform to detect the iris and pupil boundaries. Ma et al. [4,5] used the Hough transform to detect the inner and outer boundaries of the iris. In [17], Miyazawa et al. deployed a deformable iris model to locate the iris boundary. In [21], authors employed the Canny edge detection and circular Hough transform to localize the iris boundary and the local partial Hausdorff distance (PHD) was employed for comparing the binary edge maps. Most of the current iris recognition schemes process the iris images that are captured on axis. Recently, researchers have focused on the processing of nonideal iris images, which are defined as accounting for the off-angle, occluded, blurred, and noisy images. The earlier techniques for the nonideal iris recognition were not adjusted and designed specifically for the nonideal situation [9]. For the iris segmentation, most researchers assume that the iris, pupillary, and eyelid boundaries are circular or elliptical in shape [15,16]. However, it is difficult to determine the model parameters of those presumed shapes in a nonideal situation for the accurate segmentation of degraded iris images. Since the inner boundary may be partially occluded by the reflections and the outer boundary may be partially covered by the eyelids, it is important to fit the flexible contour that can stand against such disturbances. Another constraint is that the inner and outer boundary models must form a closed curve [11]. Recently, several researchers proposed different nonideal iris segmentation schemes. In [11], the inner and outer boundaries were detected in terms of active contours based on the discrete Fourier series expansions of the contour data. Two approaches were proposed in [9]; the first approach compensated for the off-angle gaze direction, and the second approach used an angular deformation calibration model. In [12,15,16], curve

Table 1 Comparison of different iris segmentation algorithms

Authors	Iris segmentation algorithms
Daugman [1–3]	Integro-differential operator
Daugman [11]	Active contours and generalized coordinates, excluding eyelashes using statistical inference
Wildes et al. [7]	Image intensity gradient and Hough transform
Bole and Boashash [6]	Edge and contour detection
Masek [36]	Canny edge detection and Hough transform
Ma et al. [4]	Gray-level information, canny edge detection and Hough transform
Ma et al. [5]	Gray-level information, canny edge detection and Hough transform
Proenca and Alexandre [13]	Integro-differential operator
Vatsa et al. [12]	Nonideal iris segmentation using Mumford–Shah functional
Miyazawa et al. [17]	Deformable iris model with 10 parameters
He et al. [21,32]	Pulling and pushing elastic approach
Liu et al. [18]	Modified Hough transform
Liu et al. [19]	Canny edge detection and Hough transform
Schuckers et al. [9]	Integro-differential operator and angular deformation model
Ross et al. [15,16]	Geodesic active contours
Sudha et al. [21]	Canny edge detection and Hough transform
Puhan et al. [39]	Fourier spectral density
Proposed approach	Game-theoretic fusion strategy that combines the complementary strengths of region-based and boundary-based methods

evolution approaches based on geometric active contours were applied to segment the nonideal iris images. In [25,27,35,38], we proposed different iris segmentation schemes based on the variational level set methods. Puhan et al. [39] proposed a segmentation scheme to localize the limbic and pupil boundaries from noisy frontal view iris images using the Fourier spectral density. Table 1 shows the comparison of different existing iris segmentation algorithms. The active contour-based segmentation approaches reported in [11,12,15,16] produce a good fit and handle the discontinuities in contour data; however, the performance of those approaches may be deteriorate due to the effects of weak iris/sclera boundary, nonuniform intensity, and low image contrast since each of these schemes uses only the boundary-based information for iris localization. Also, the parametric active contour-based iris segmentation scheme proposed in [11] may terminate at a certain local minima such as the specular reflections, the thick radial fibers in the iris, or the crypts in the ciliary region. Also, the technique reported in [11] depends on the order of the Fourier series to approximate the inner and outer boundaries of the iris. However, the order of the two boundaries may be different. Thus, selecting the order of the Fourier series is a difficult task [16]. The curve evolution approaches deployed in [12,15,16,27] depend on the value of the gradient for the boundary points and thus may suffer from the noise sensitivity. Also, the approach proposed in [38] may be affected by poor localization and over-segmentation. Addressing the above problems, a game theory (GT)-based fusion scheme is deployed to accurately extract the iris from the surrounding structures in an iterative fashion. Game-theoretic methods have been used in the field of medical image analysis to segment MRI images of the heart and brain and also to rank the best features from the extracted feature sequence of relatively higher dimension [51]. Furthermore, GT has been used extensively in wireless networks research to develop the understanding of stable operation points for networks. In this research effort, their significance in the context of nonideal iris segmentation is demonstrated.

3 Iris segmentation algorithm

In this paper, we propose a three-stage iris segmentation algorithm, in which we first apply a noise removal scheme to reduce the effects of specular reflections and eyelashes, and the second stage provides an initial approximation of the center point of the pupil by using the direct least square (DLS) [47]-based elliptical fitting. In the third stage, we apply a parallel game-theoretic decision making procedure by modifying the Chakraborty and Duncan's algorithm [45,46], which combines the region-based segmentation and the boundary-finding methods for the optimal estimation of the inner and the outer boundaries. To improve the quality of the iris image, we apply a local histogram equalization technique, and to suppress the effect of noise, we deploy the 2D Wiener filter to the equalized images [48].

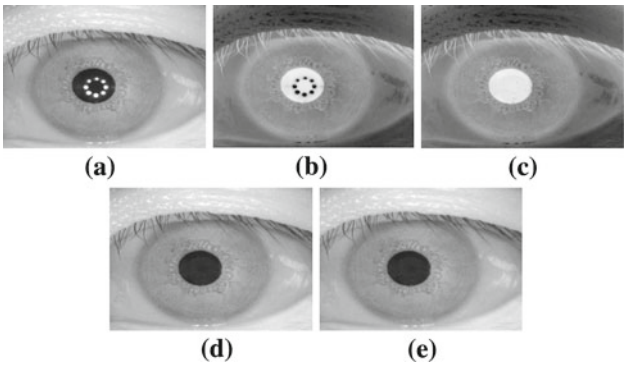

Fig. 2 Image preprocessing on CASIA Version 3 data set. **a** original image, **b** complement of the image, **c** filling the holes, **d** complement of image (**c**), **e** image after Gaussian smoothing

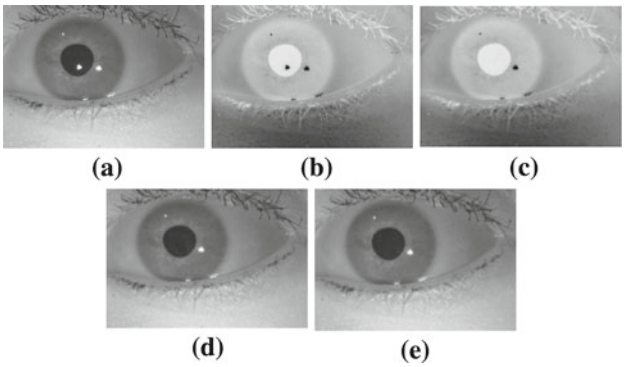

Fig. 3 Image preprocessing on WVU data set. **a** original image, **b** complement of the image, **c** filling the holes, **d** complement of image (**c**), **e** image after Gaussian smoothing

3.1 Specular reflection detection and iris boundary approximation

In the first stage of iris segmentation, we remove the specular reflection spots that are found inside the pupillary region (see Figs. 2a, 3a) and these white spots may cause a false inner boundary detection and may also halt the region-growing process prematurely. To remove these spots, first we complement the input iris image by taking the absolute subtraction of each pixel's intensity level from 255, then, we fill the dark holes found in the pupillary region in the complemented iris image. A "hole" is the set of dark pixels surrounded by light pixels that cannot be reached from the edge of the image. We adopt the connectivity of 4 pixels on the background pixels. Finally, we complement the processed image again and apply the Gaussian filter to smoothen the resulted sharp image. This process is illustrated in Figs. 2 and 3. The accuracy of the DLS-based ellipse fitting process degrades in the presence of outliers such as the eyelashes. Therefore, we apply a morphological operation, namely the opening, to the preprocessed iris image to suppress the interference of the eyelashes. In the second stage, we deploy a DLS-based elliptical fitting to

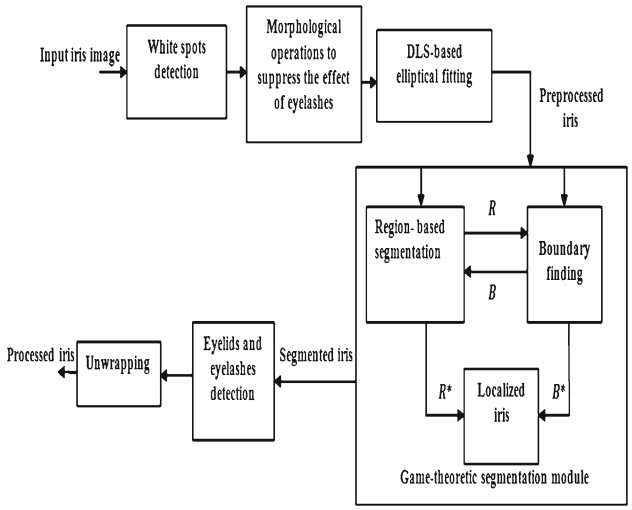

Fig. 4 Flow diagram of the proposed iris segmentation scheme. Game-theoretic segmentation module integrates the region-based segmentation and boundary-finding methods

approximate the pupil boundary [47]. The DLS-based elliptical fitting returns five parameters $(p_1, p_2, r_1, r_2, \varphi_1)$: the horizontal and vertical coordinates of the pupil center (p_1, p_2), the length of the major and minor axes (r_1, r_2), and the orientation of the ellipse φ_1. This method, thus, provides a rough estimation of pupil boundary.

3.2 Iris and pupil detection using game theory

In the final stage, we apply a parallel game-theoretic decision making approach based on the modified Chakraborty and Duncan's method for the exact estimation of the iris/pupil boundary [45,46]. In this effort, a fully bidirectional framework is developed for integrating the boundary-finding and the region-based segmentation schemes and this leads to a system where the two schemes can operate in parallel, so that at each step, the output of each scheme gets updated using information from the outputs of both the schemes from the previous iteration and the data itself. Thus, as the game progresses, both the schemes improve their positions through a mutual information sharing (See Fig. 4). It is found that neither the boundary-finding nor the region-based segmentation by themselves is able to provide us with all the necessary information for an accurate segmentation; this is because, while the region-based segmentation is not likely to give us a precise information regarding the shape and location, the boundary-finding may not be feasible if some of the structures are not well located. Therefore, it is expected that a game-theoretic fusion of the two methods can perform better than either of the methods alone, by integrating the complementary strengths of these individual schemes. The game is played out by a set of decision makers (or "players"), which in our case corresponds to the two segmentation schemes,

namely the region-based and the gradient-based boundary-finding methods. The iris segmentation problem can be formulated as a two-player game according to [45]. If p^1 is the set of strategies of the player 1 and p^2 is the set of strategies of the player 2, then each player tries to minimize the payoff function, $F^i(p^1, p^2)$. The main objective is to find the *Nash Equilibrium* (NE) of the system $(\bar{p}^1, \bar{p}^2)$ such that

$$F^1(\bar{p}^1, \bar{p}^2) \leq F^1(p^1, \bar{p}^2), \quad F^2(\bar{p}^1, \bar{p}^2) \leq F^2(\bar{p}^1, p^2). \tag{1}$$

If we move toward the NE iteratively by taking t as the time index, we can formulate the game as:

$$p^1_{t+1} = \underset{p^1 \in P^1}{\arg\min} F^1\left(p^1, p^2_t\right); \quad p^2_{t+1} = \arg\min F^2(p^1_t, p^2) \tag{2}$$

Chakraborty and Duncan [45] proved that there always exists a NE solution if F^1 and F^2 are of the following form:

$$F^1(p^1, p^2) = f_1(p^1) + \alpha f_{21}(p^1, p^2) \tag{3}$$

$$F^2(p^1, p^2) = f_2(p^2) + \beta f_{12}(p^1, p^2) \tag{4}$$

where α and β are scaling constants, F^i is bounded in $p^i \in P^i$ F^i is continuously second-order differentiable in $p^i \in P^i$, and there exists a closed neighborhood $u^i \subseteq p^i$ such that F^i is strongly convex in u^i. Based on the above assumptions, Chakraborty and Duncan [45] provided the following theorem: For the payoff functions $F^1(p^1, p^2)$ and $F^2(p^1, p^2)$, there exists a locally stable NE solution. For any $p^1 \in U^1 \subseteq P^1$ and $p^2 \in U^2 \subseteq P^2$, the sequence of rational choices generated by the parallel decision making process converges and the limit point is NE solution if α and β satisfy the following condition [45]:

$$\left\| \left[\left(\alpha^{-1} \frac{\partial^2}{\partial p^1 \partial p^1} f_1(p^1) + \frac{\partial^2}{\partial p^1 \partial p^1} f_{21}(p^1, p^2) \right)^{-1} \frac{\partial^2}{\partial p^1 \partial p^2} f_{21}(p^1, p^2) \right) \right] \times \left[\left(\beta^{-1} \frac{\partial^2}{\partial p^2 \partial p^2} f_2(p^2 \right) + \frac{\partial^2}{\partial p^2 \partial p^2} f_{12}(p^1, p^2) \right)^{-1} \left(\frac{\partial^2}{\partial p^2 \partial p^2} f_{12}(p^1, p^2) \right) \right] \Bigg\| < 1.$$

In the region-based method, the iris image is partitioned into connected regions by grouping the neighboring pixels of similar intensity levels. The adjacent regions are then merged under some criteria involving the homogeneity or sharpness of the region boundaries. Now, if $y_{i,j}$ is the intensity of a pixel at (i, j) of the original image and $x_{i,j}$ is the intensity of a pixel at (i, j) of the segmented image, then a common approach is to minimize an objective function of the form:

$$E = \sum_{(i,j)} \left(y_{i,j} - x_{i,j}\right)^2 + \lambda \left(\sum_{i,j} \sum_{i_s, j_s} \left(x_{i,j} - x_{i_s j_s}\right)^2 \right). \tag{5}$$

where i_s and j_s are indices in the neighborhood of pixel $x_{i,j}$ and λ is a constant. In the above equation, the first term of the right-hand side is a data fidelity term and the second term enforces the smoothness. Therefore, the first term tries to minimize the difference between the classification and the pixel intensity. The second term minimizes the difference between the classifications of the neighboring pixels, essentially to minimize the region boundary. To detect the inner/outer boundary of the iris, the objective functions are as follows:

For the region-based module (player 1),

$$F^1\left(p^1, p^2\right) = \min_x \left[\sum_{i,j} \left(j_{i,j} - x_{i,j}\right)^2 + \lambda^2 \left(\sum_{i,j} \left(x_{i,j} - x_{i-1,j}\right)^2 + \sum_{i,j} \left(x_{i,j} - x_{i,j-1}\right)^2 \right) \right] + \alpha \left[\sum_{i,j \in A\tilde{p}} \left(x_{i,j} - u\right)^2 + \sum_{i,j \in \bar{A}\tilde{p}} \left(x_{i,j} - v\right)^2 \right] \tag{6}$$

where $y_{i,j}$ is the intensity of the original image, $x_{i,j}$ is the intensity of the segmented image given by p^1 as mentioned before, u is the intensity inside the contour given by p^2, and v is the intensity outside the contour given by p^2. The first term on the right-hand side of (6) minimizes the difference between the pixel intensity values and the obtained region, as well as enforces continuity. The second term tries to match the region and the contour. In the region-growing approach, we select an initial seed that is a single pixel within the region of interest for the inner boundary detection. At each iteration, the neighboring pixels are observed and the value of E is measured from (5). The pixels, for which the value of E is less than a predefined threshold, are accepted into the region.

The objective function of the player 2 (i.e., the boundary-finding module) is as follows:

$$F^2\left(p^1, p^2\right) = \underset{\vec{p}}{\arg\max} \left[M_{\text{gradient}}\left(I_g, \vec{p}\right) + \beta M_{\text{region}}(I_r, \vec{p}) \right] \tag{7}$$

where $\vec{p}$ denotes the parameterization of the contour given by p^2, I_g is the gradient image, I_r is the region-segmented image, and β is a constant. In [45], the Fourier parameterization was used to represent the evolving contour. However, the

parametric active contour-based curve evolution may terminate at a certain local minima such as the specular reflections, the thick radial fibers in iris, or the crypts in the ciliary region and thus is not suitable for nonideal iris boundary detection. Therefore, we apply a level set-based active contour model to represent the contour data [27,40–44]. Also, the contours represented by the level set may break and merge naturally during evolution, and thus, the topological changes are handled automatically. The proposed level set-based methods are discussed briefly in the following subsection.

3.2.1 Acquiring iris/pupil contour data using level set methods for game-theoretic curve evolution process

In order to obtain the contour data of the inner (pupil) boundary during game-theoretic evolution, we apply the geometric active contours based on the edge stopping function with the assumption that the pupillary region is the darkest part of the eye and is separated by relatively a strong gradient from the iris region [27]. Let Ω be the image domain and I be the two-dimensional iris image. Let us consider the evolving curve C in Ω, as the boundary of an open subset ω of Ω. The main idea is to embed this evolving curve as the zero level set of a higher-dimensional function ϕ. We can define the following function:

$$\phi(x, y, t = 0) = \pm d \tag{8}$$

where d denotes the distance from (x, y) to C at time $t = 0$. The plus (minus) sign is selected if the point (x, y) is outside (inside) the curve C. Therefore, in the curve evolution approach for obtaining pupil contour data, we need to solve the *partial differential equation* (PDE) of the following form

$$\frac{\partial \phi}{\partial t} = g(I)\left(S_1\left|\nabla_\phi\right| + S_2\left|\nabla_\phi\right|\right), \phi(x, y, 0) = \phi_0(x, y) \tag{9}$$

where S_1 is a constant advection term that forces the curve to expand or contract uniformly based on the its sign, S_2 depends on the curve geometry and is used to smooth out the high-curvature region, the set $\{(x, y), \phi_0(x, y) = 0)$ defines the initial contour, and $g(I)$, an edge stopping function, which is used to halt the evolution of the curve at the inner boundary, can be defined as:

$$g(I) = \frac{1}{1 + |\nabla G_\sigma(x, y) * I(x, y)|^\rho}, \quad \rho \geq 1 \tag{10}$$

where $G_\sigma(x, y) * I(x, y)$ is the convolution of I with the Gaussian $G_\sigma(x, y) = \sigma^{-1/2} e^{-|x^2+y^2|/4\sigma}$. Now to discretize ϕ, we apply the finite differences scheme proposed in [41]. To evolve the curve, we perform the discretization and linearization of (9) [41,43]:

$$\emptyset_{i,j}^{n+1} = \emptyset_{i,j}^{n} - \Delta t\left[\hat{g}(I)\left(\hat{s}_1\left|\nabla_\phi\right| + \hat{s}_2\left|\nabla_\phi\right|\right)\right] \tag{11}$$

where Δ_t is the time step, (x_i, y_j) are the grid points for $1 \leq i, j \leq M$, and $\phi_{i,j}^n = \phi(x_i, y_j, n\delta t)$ approximates $\phi(x, y, t)$ with $n \geq 0$, $\phi^0 = \phi_0$. In [43], an upwind scheme is used to estimate $s_1\left|\nabla_\phi\right|$ of (9):

$$\begin{aligned} s_1|\nabla_\phi| = \Big[&\max\left(\Delta_-^x \phi_{i,j}^n, 0\right)^2 + \min\left(\Delta_-^x \phi_{i,j}^n, 0\right)^2 \\ &+ \max\left(\Delta_-^y \phi_{i,j}^n, 0\right)^2 + \min\left(\Delta_-^y \phi_{i,j}^n, 0\right)^2\Big]^{1/2} \end{aligned} \tag{12}$$

and the term $s_2\left|\nabla_\phi\right|$ depends on curvature K ($K = \operatorname{div}\left(\frac{\nabla_\phi}{|\nabla_\phi|}\right)$) and can be estimated as:

$$\begin{aligned} s_2\left|\nabla_\phi\right| = -\epsilon K\Big[&\left(\phi_{i+1,j}^n - \phi_{i-1,j}^n/2\right)^2 \\ &+ \left(\phi_{i,j+1}^n - \phi_{i,j-1}^n/2\right)^2\Big] \end{aligned} \tag{13}$$

where ϵ is a constant.

In order to acquire the contour data for the outer boundary during game-theoretic segmentation process, we use modified Mumford-Shah segmentation model with the regularization terms using the energy minimization algorithm [40,42]. The level set approach with the energy minimization algorithm provides the outer boundary data accurately during GT-based progression by considering the fact that the iris and sclera may not be separated by a strong gradient. Therefore, the main objective is to minimize the length of the curve and the area of the region inside the curve. We introduce the following energy function:

$$\begin{aligned} &E(C, c_1, c_2) \\ &= \mu \int_\Omega \delta(\phi(x, y))|\nabla_\phi(x, y)|\mathrm{d}x\mathrm{d}y \\ &\quad + v \int_\Omega H(\phi(x, y))\mathrm{d}x\mathrm{d}y \\ &\quad + \lambda_1 \int_\Omega |I(x, y) - c_1|^2 H(\phi(x, y))\,\mathrm{d}x\mathrm{d}y \\ &\quad + \lambda_2 \int_\Omega |I(x, y) - c_2|^2 (1 - H(\phi(x, y)))\,\mathrm{d}x\mathrm{d}y \end{aligned} \tag{14}$$

where $\mu \geq 0$, $v \geq 0$, $\lambda_1 > 0$, $\lambda_2 > 0$ are the positive constants, C is the evolving curve, c_1, c_2 are the averages of iris image I inside and outside of C, respectively, ϕ denotes the zero level set of the signed distance function representing C as in (8), H is the Heaviside function, and δ is the Dirac measure. In (14), the first and the second terms denote the area

and length at $\phi = 0$, respectively. Therefore, the main goal is to estimate the values of C, c_1, c_2 such that $E(C, c_1, c_2)$ is minimized. We parameterize the descent direction by $t \geq 0$ and deduce the Euler–Lagrange PDE from (14) which leads to the following active contour model:

$$\phi_t' = \delta(\phi)\left[\mu \,\mathrm{div}\,\left(\nabla_\phi/|\nabla_\phi|\right) - v - \lambda_1(I - c_1)^2 + \lambda_2(I - c_2)^2\right]. \tag{15}$$

Now, we regularize the Heaviside function H and the Dirac measure δ as in [43]:

$$H_\epsilon(\phi(x, y)) = \frac{1}{2} + \frac{1}{\pi}\arctan\left(\frac{\phi(x, y)}{\epsilon}\right) \quad \text{and} \quad \delta(\phi(x, y)) = \frac{1}{\pi}\cdot\frac{\epsilon}{\epsilon^2 + (\phi(x, y))^2}. \tag{16}$$

From (16), we can observe that the evolution scheme has the tendency to measure the global minimizer with the applied regularizations. By discretizing and linearizing (14), we obtain:

$$\frac{\phi_{i,j}^{n+1} - \phi_{i,j}^{n}}{\Delta t} = \delta_\epsilon\left(\phi_{i,j}^{n}\right)\left[\mu\, K - v - \lambda_1\left(I_{i,j} - c_1(\phi^n)\right)^2 + \lambda_2\left(I_{i,j} - c_2(\phi^n)\right)^2\right]. \tag{17}$$

Now, to get the contour data for game-theoretic localization process, we initialize the active contour, ϕ just beyond the pupil boundary to obtain the approximate information about the iris contour.

In our game-theoretic implementation, we simplify the approach proposed in [45] by excluding the prior shape information with the assumption that the inner and outer boundaries of the iris images of the underlying nonideal iris data sets do not maintain a particular shape. In order to estimate the exact boundary of the pupil, we deploy the game-theoretic segmentation algorithm mentioned above and use the center of the pupil obtained through the DLS-based elliptical-fitting process as the seed point. The pupil segmentation results are shown in Figs. 5 and 6. Similarly, for computing the exact estimate of the outer boundary, we apply again a segmentation scheme based on the noncooperative game theory, and here, we select a circular region of radius r, which is found in the previous step, just beyond the pupillary boundary so that the game-theoretic localization scheme moves toward the outer boundary from this region. This process is shown in Figs. 7 and 8.

3.3 Noise detection, unwrapping, and enhancement

We deploy the eyelids and the eyelashes detection techniques as used in our previous works [25,27,35,37,38]. We use a mask based on the extracted eyelids and eyelashes to detect the iris region without noise. In order to compensate for the

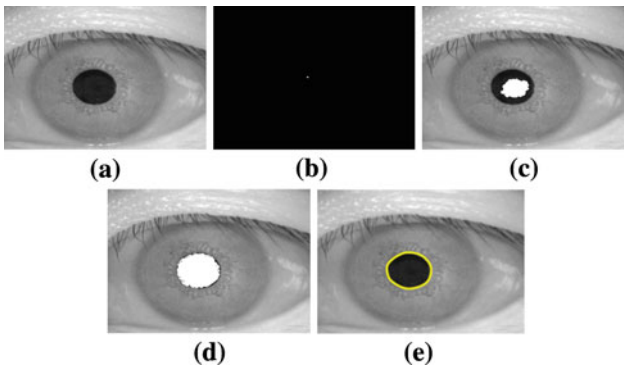

Fig. 5 Pupil segmentation using game-theoretic integration approach on CASIA Version 3 data set. **a** Preprocessed image, **b** seed image, **c** and **d** game-theoretic region growing process and boundary-finding method, **e** final contour of pupil

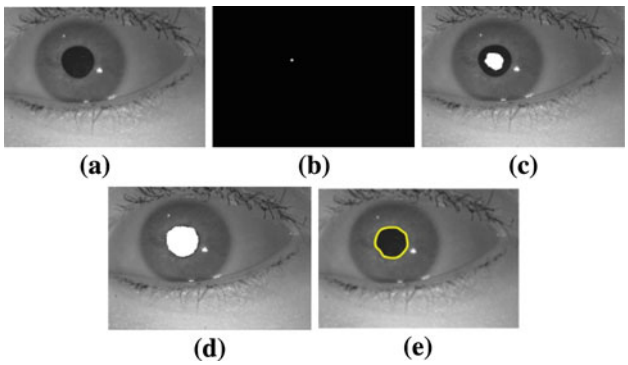

Fig. 6 Pupil segmentation using game-theoretic integration approach on WVU data set. **a** Preprocessed image, **b** seed image, **c** and **d** game-theoretic region growing process and boundary-finding method, **e** final contour of pupil

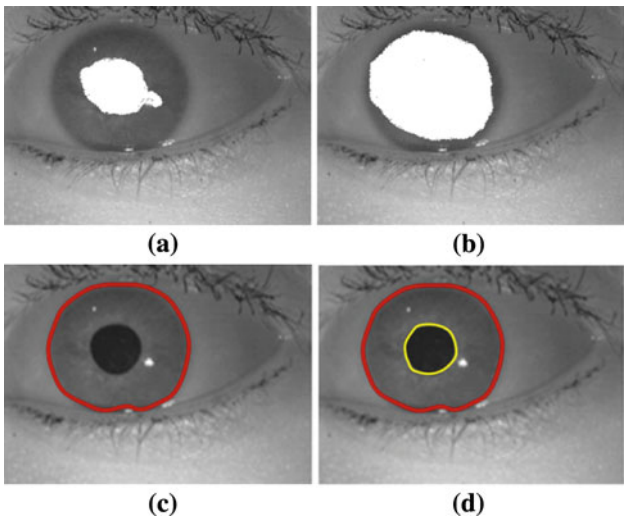

Fig. 7 Iris segmentation using game-theoretic integration approach on WVU data set. **a** Iris segmentation starts just beyond the previously obtained pupil boundary, **b** game-theoretic region growing process, **c** final contour of the iris, **d** final contours of iris and pupil

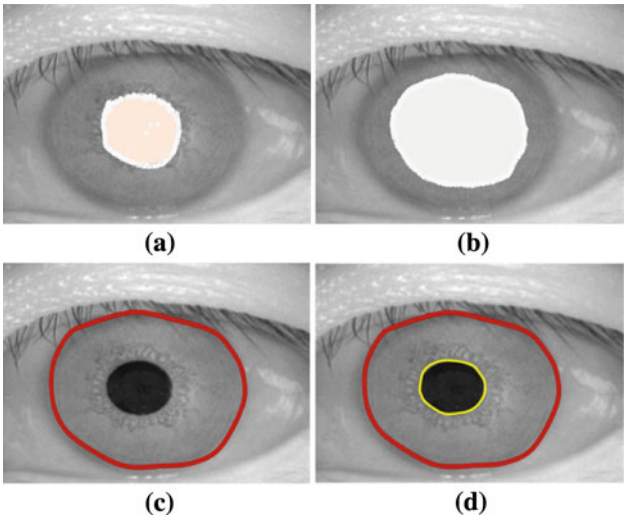

Fig. 8 Iris segmentation using game-theoretic integration approach on CASIA Version 3 data set. **a** Iris segmentation starts just beyond the previously obtained pupil boundary, **b** game-theoretic region growing process, **c** final contour of the iris **d** final contours of iris and pupil

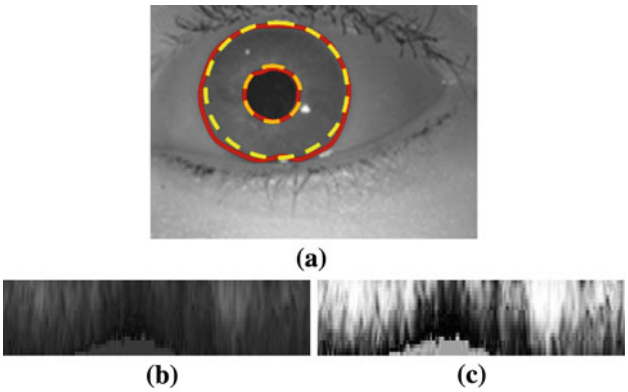

Fig. 9 Unwrapping and enhancement. **a** estimated iris/pupil boundary, **b** unwrapped iris image, **c** enhanced iris image

elastic deformation in iris texture, we unwrap the extracted (and localized) iris region to a normalized rectangular block of fixed size 64 × 514 by converting from the Cartesian coordinates to the polar coordinates using the circle-fitting strategy deployed in [16]. Figure 9a indicates the estimated iris/pupil boundary, and Fig. 9b shows the normalized image. In order to improve the quality of the iris image, we have applied a two-step image enhancement technique:

Step 1: Since the normalized iris image has a relatively low contrast and may have nonuniform intensity values due to the position of the light sources, a local intensity-based histogram equalization technique is applied to enhance the quality of the contrast of the normalized iris image, thereby increasing the subsequent recognition accuracy. In our method, a local cumulative histogram is applied to the image subblock of size 10 × 10 centered at the pixel to be converted.

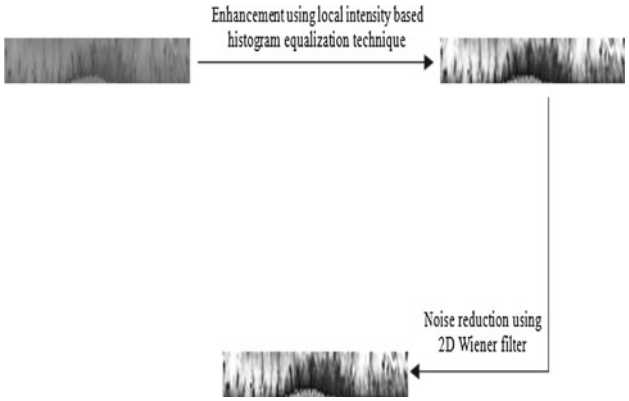

Fig. 10 Contrast Enhancement using local cumulative histogram equalization technique and noise reduction with 2D Wiener filter

Step 2: To reduce the effect of noise, we apply a pixel-wise adaptive 2D Wiener filter [48]. The 2D Wiener filter is a low-pass filter that is used to remove the high-frequency noise. This filter emphasizes on the local statistics estimated from a local neighborhood, η of size 3 × 3 of each pixel, and is defined by:

$$\mathrm{WF}(n_1, n_2) = \mu + \frac{\left(\sigma^2 - v^2\right)}{\sigma^2} * (I(n_1, n_2) - \mu) \tag{18}$$

where v^2 denotes the noise variance, μ and σ^2 are the local mean and variance, I is the gray-level intensity in $n_1, n_2 \in \eta$. If the noise variance is not provided, it uses the average of all the local estimated variances. Figures 9c and 10 also show the effects of the enhancement on the normalized iris images.

3.4 Feature encoding and matching

In this paper, the Daubechies wavelet transform (DBWT) is applied to extract the characteristics values from the normalized (and enhanced) image block of size 64 × 512 pixels as applied in our early work [25,38], and this technique is well suited for analyzing the signals in the multi-resolution mode [49,50]. In this paper, we use Hausdorff distance (HD) for iris templates matching. The HD is used to measure the dissimilarity between two sets of feature points. If $A = \{a_1, a_2, a_3, \ldots, a_m\}$ and $B = \{b_1, b_2, b_3, \ldots, b_n\}$ are two sets of iris features, the *HD* between A and B is given by [21,27]:

$$H(A, B) = \max(h(A, B), h(B, A)) \tag{19}$$

where h is the directed Hausdorff defined by: $h(A, B) = \max_{a_i \in A} \min_{b_i \in B} \|a_i - b_i\|$ and $\|\cdot\|$ is the norm of the vector.

4 Experimental results and discussions

In this section, we report the results of a set of experiments to evaluate the performance of the proposed scheme and then summarize our findings. Our experimentation is conducted in two stages: first, we evaluate the performance of our proposed algorithms with respect to the game-theoretic segmentation scheme, and second, we compare the performance of our approach with those of the other state-of-the-art algorithms to show the effectiveness of the proposed scheme. Extensive experiments on different iris image data sets are conducted to evaluate the performance in two modes: the verification (one-to-one) and the identification (one-to-many). In the verification mode, we measure the performance in terms of the *Genuine Accept Rate (GAR)*, *False Accept Rate (FAR)*, and *Equal Error Rate (EER)* [10] with the assumption that a test sample is from a specific subject. In the identification mode, we make a one-to-many search in the entire data set for a given test sample to find the highest matched template with that test sample. Thus, for the identification, we use the standard measure *correct recognition rate (CRR),* which is defined as follows:

$$\text{CRR} = \frac{\text{Correctly recognized use rnumber}}{\text{Total number of users enrolled}} \times 100. \qquad (20)$$

4.1 Data sets used

The extensive experimentation is conducted on four data sets, namely the ICE 2005 [52], the CASIA Version 3 [53], the UBIRIS Version 1 [54], and WVU Nonideal [55]. We have selected the aforementioned data sets for the performance evaluation since these data sets contain nonideal iris images including off-angle, occluded, blurred, and noisy images that are acquired with different devices under varying conditions to facilitate a comprehensive performance evaluation in a real-word application level scenario. These data sets also represent different ethnicities [12].

The ICE 2005 [52] iris data set contains 2,953 images corresponding to 244 classes. The ICE data set consists of left and right iris images for experimentation (1,528 left iris images from 120 classes and 1,425 right iris images from 124 classes). This data set is divided into two categories: the "gallery" images, which are considered as good quality images, and the "probe" images, which represent iris images of varying quality. The iris images are intensity images with a resolution of 640 × 480. The average diameter of an iris is 228 pixels.

The CASIA Version 3 [53] iris data set includes 2,655 iris images from 249 different persons, with 396 iris classes. Most of the images are captured in two sessions with at least one month interval. The iris images are 8-bit gray-level images with a resolution of 320 × 280.

The UBIRIS Version 1 [54] data set contains 2,410 iris images from 241 classes. The iris images are captured in two sessions. The iris images captured in the first session represent the good quality images whereas the images in the second session have the irregularities with respect to focus, intensity, and reflection.

The WVU Nonideal [55] iris data set contains 800 images corresponding to 200 classes. Each class is represented by four images collected at three angles on the order of 0°, 15°, 30°, and again 0°. The iris images are intensity images with a resolution of 640 × 480.

The combined nonhomogeneous data set—In order to perform an extensive experimentation and to validate our proposed approach, we generate a nonhomogeneous data set by combining the above four data sets and this data set consists of 8,818 images corresponding to 1,081 classes.

4.2 Performance evaluation of the proposed scheme

To validate the performance of the proposed algorithms, we carry out the experimentation on four data sets mentioned above. For the iris segmentation, we apply the game-theoretic integration approach and the segmentation results are shown in Figs. 11 and 12. We find from the Figs. 11 and 12 that our segmentation scheme performs well despite the fact that the iris and the sclera regions are separated by a blurred boundary especially in the UBIRIS and WVU data sets. Based on the extensive experimentations, the coupling coefficients, α and β are set to 0.27 for all the data sets when the game-theoretic integration module is used. To obtain the contour data of the inner boundary with the edge-stopping function for boundary-based module during game-theoretic evolution, the selected parameters values are set to $\Delta_t = 0.05$ and constant, $\epsilon = 0.015$. The selected parameters values to obtain

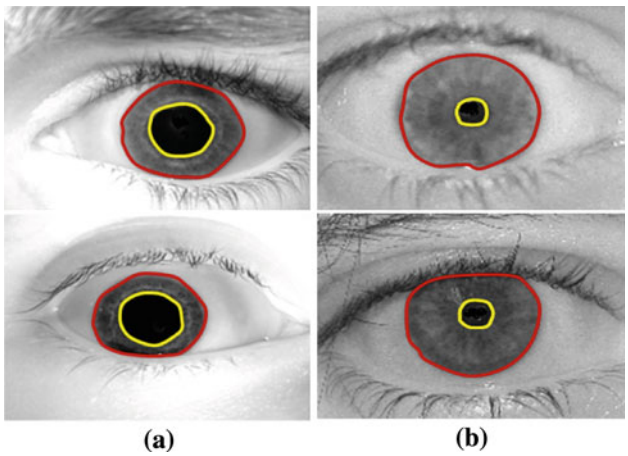

Fig. 11 Segmentation results on data sets. **a** ICE 2005, and **b** UBIRIS Version 1

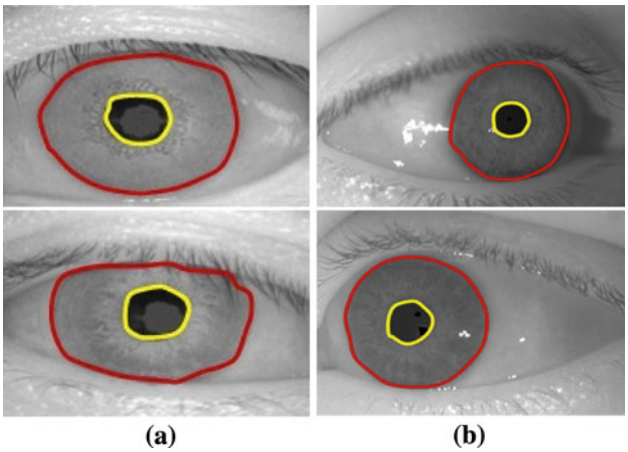

Fig. 12 Segmentation results on data sets. **a** CASIA Version 3, and **b** WVU Nonideal

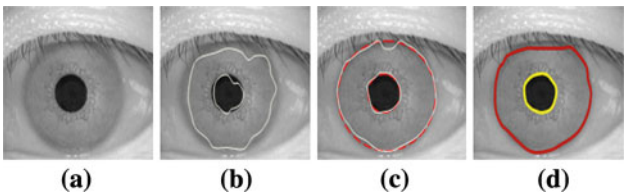

Fig. 13 Effectiveness of our proposed segmentation scheme based on game-theoretic fusion on a sample iris image from CASIA Version 3 data set. **a** Original image, **b** output of the region-based approach without game-theoretic approach (only final contours are shown), **c** output of the boundary-finding approach without game-theoretic approach, The *red* contour denotes the initialization using the DLS-based elliptical fitting for level set-based curve evolution and the white contour denotes the final output for inner and outer boundaries, **d** output with proposed game-theoretic integration

the iris contour data using energy minimization algorithm for boundary-based module of game-theoretic propagation are set to $\mu = 0.00001, \upsilon = 0.02, \lambda_1 = \lambda_2 = 1, \Delta t = 0.1$ and constant, $\epsilon = 1$. Comparisons are first made between the outputs generated using the game-theoretic fusion and the corresponding outputs obtained without using the information integration. Equations (6) and (7) jointly represent the outputs of the game-theoretic fusion, where (6) provides the region output and (7) gives the boundary output under the integrated framework. For the stand-alone modules, the coupling coefficients, α and β are set to 0. From Fig. 13, it is clear that the final contour output shown in Fig. 13d with the information fusion is much better than the outputs of the stand-alone modules shown in Fig. 13b and c, where no information fusion is deployed. Our proposed segmentation scheme is also robust in noisy situations. A sudden variation in the intensity level may occur in the iris image due to a noisy pixel, and thus, the moving front may stop. However, in our case, the other boundary points continue to move, and hence, the curve evolution process based on game-theoretic fusion keeps propagating toward the inner

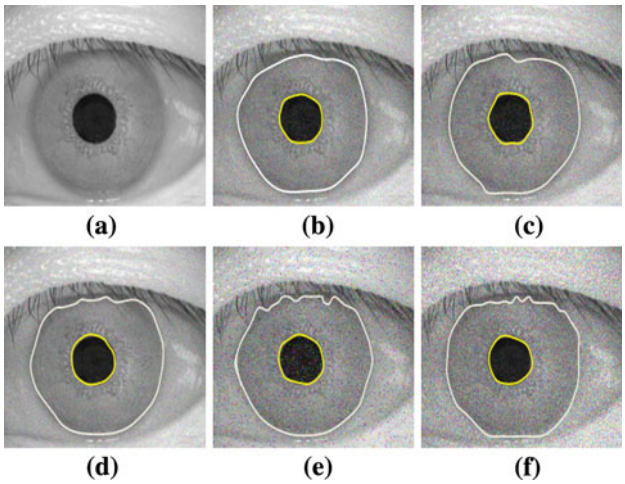

Fig. 14 Performance of our game-theoretic algorithm in noisy situations. **a** Original image after filling the *white spots* from CASIA Version 3 data set, **b** Gaussian white noise (mean = 0 and variance = 0.005), **c** Gaussian white noise (mean = 0 and variance = 0.007), **d** iris image with Poisson noise, **e** iris image with salt and pepper noise (noise density = 0.06), **f** iris image with speckle noise which adds the multiplicative noise (mean = 0 and variance = 0.07)

and the outer boundaries. Figure 14b and c shows the outputs of applying our proposed game-theoretic scheme to an iris image with Gaussian white noise. Figure 14d–f shows the results of applying our approach to an iris image with the Poisson noise, the salt and pepper noise, and the speckle noise, respectively.

One major advantage of our algorithm when compared to the methods proposed in [15,16] is the use of topology preserving technique instead of standard geodesic active contours. Therefore, even in the noisy situations, our proposed approach can localize the inner and outer boundaries accurately. In order to exhibit the effectiveness of our segmentation approach, we compare our GT-based approach with the integro-differential operator (IDO) proposed by Daugman [1], the Canny edge detection and Hough transform (CHT)-based approach applied in our previous work [26], and the active contour-based localization approaches proposed by Vatsa et al. [12] and Ross et al. [15,16] for all the data sets. For the comparison purpose, we only implement the segmentation approaches proposed in [1,12,15,16]. The ROC curves in Fig. 15 show that the matching performance is improved when the game-theoretic integration is used for segmentation. The proposed segmentation scheme shows a better performance than the active contour-based methods reported by Vatsa et al. [12] and Ross et al. [15,16], and the reason is that our proposed scheme uses the region-based information as well as the gradient data with the game-theoretic fusion method. Moreover, a morphological operation and a white spot detection technique are applied to an input image to restrain the interference from the eyelashes prior to deploying

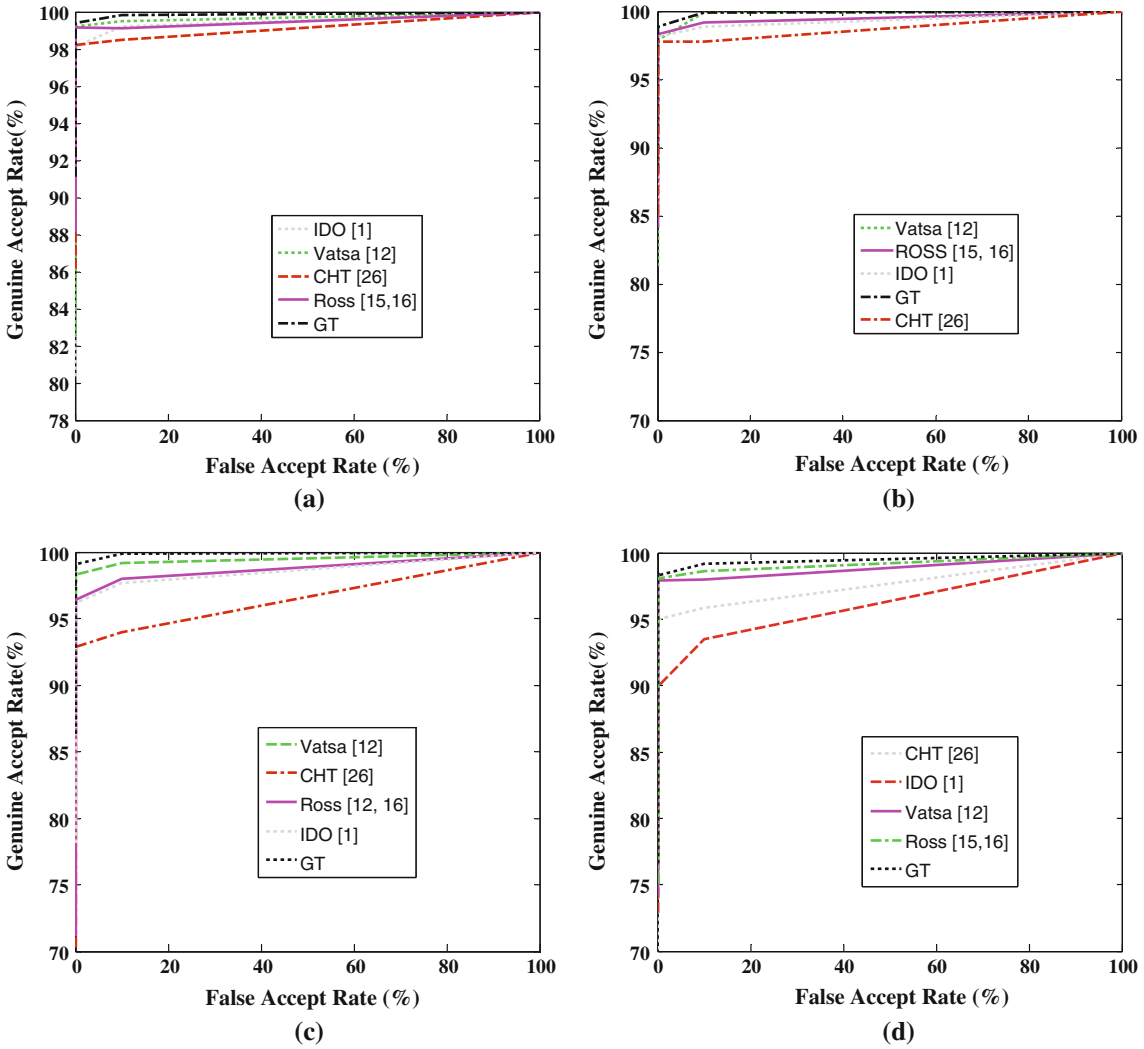

Fig. 15 ROC curves show the comparison of different existing segmentation techniques on **a** ICE 2005, **b** UBIRIS Version 1, **c** CASIA Version 3, and **d** WVU nonideal data sets

the DLS-based elliptical fitting and also to suppress the effect of reflections occurred inside the pupil. The DLS-fitting approach provides a reasonable approximation of the inner boundary. The GAR at a fixed FAR of 0.001% is (a) 98.15% in ICE, (b) 97.17% in CASIA, (c) 97.24% in UBIRIS, and (d) 96.31% in WVU data sets. In order to show the robustness of the game-theoretic approach, we also compare the proposed segmentation algorithm with the region-based active contour model (RAC) [38] and level set (LS)-based [27] methods, which were proposed in our early works. We find from Fig. 16 that our algorithm achieved the highest GAR of 97.12% on the combined data set at the fixed FAR of 0.001%. Furthermore, we also provide the EERs of each of the schemes in Fig. 16 and our proposed segmentation scheme effectively increases the performance with the EER of 0.86%. The reason seems to be the inclusion of both the

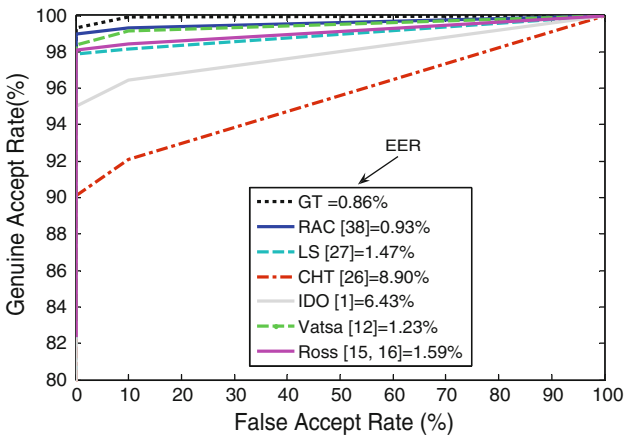

Fig. 16 ROC curves show the comparison of different existing segmentation techniques on the combined data set

Fig. 17 Sample of iris images from UBIRIS Version 1 data set [54] on which the proposed segmentation scheme fails to detect the iris/pupil boundary

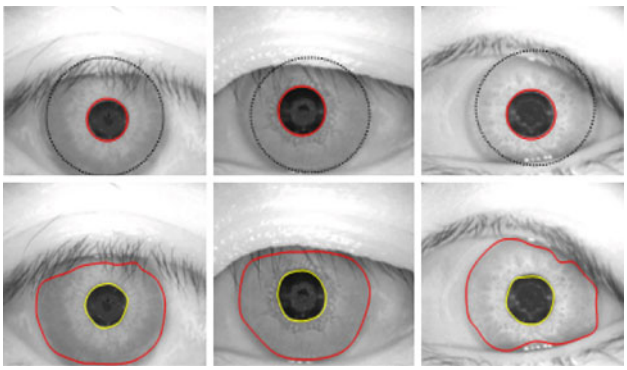

Fig. 18 Sample of iris images from CASIA Version 3 data set [53] on which the DLS elliptical-fitting approach fails to detect outer boundary accurately (*upper row*). However, our proposed game-theoretic segmentation approach successfully isolates the inner and boundaries for the corresponding images (*lower row*)

region-based and boundary-based information for segmentation, whereas the schemes reported in [1,12,15,16,27] used only the gradient information, and the segmentation algorithm depicted in [38] used only the region data. Therefore, the localization algorithms of [1,11,12,15,16,27] may suffer from noise sensitivity and blurred iris/sclera boundary, on the contrary, the approach in [38] seems to experience poor localization and over-segmentation. However, the proposed game theory-based segmentation algorithm fails to perform on some images of UBIRIS data set due to huge occlusion as shown in Fig. 17. For experimental purpose, we also apply the DLS-based elliptical-fitting approach to detect the outer boundary as well as the inner boundary and Fig. 18 exhibits that the DLS elliptical-fitting strategy fails to detect the outer boundary accurately; however, the game-theoretic localization process isolates the iris and pupil boundaries accurately in those corresponding cases. Therefore, we observe from our experimentation that the elliptical-fitting process alone cannot provide an optimal estimation of the iris boundary. In Fig. 19, we also find that segmentation error occurs on several iris images due to poor quality of the images, huge occlusions, and the deviated gaze. We conducted the above experimentation on a 3.00 GHz Pentium IV PC with 2.5 GB

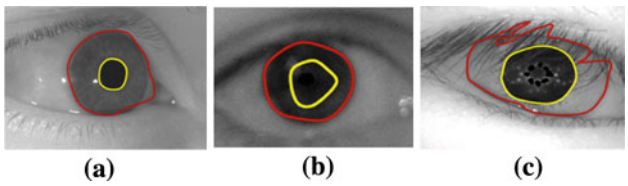

Fig. 19 Segmentation errors found on several images of **a** WVU non-ideal, **b** UBIRIS Version 1, and **c** CASIA Version 3 data sets using game-theoretic approach

Table 2 Average time consumption of different parts of the proposed iris recognition system

Algorithm	Time (ms)
Iris segmentation	793
Unwrapping	83
Feature extraction	72
Matching	38
Average execution time	986

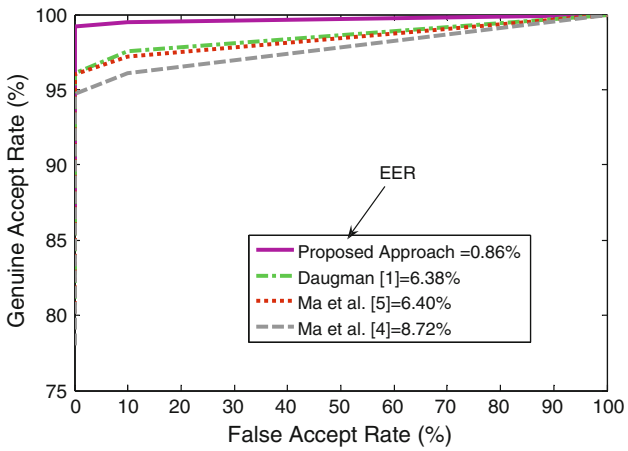

Fig. 20 Comparison with existing iris recognition schemes on the combined data set

RAM in MATLAB 7.2 environment. The average time consumption of matching an iris image is 986 ms as exhibited in Table 2.

4.3 Comparison with the other state-of-the-art algorithms

We compare the performance of the proposed algorithm with the other existing iris recognition algorithms. We implement the well-known iris recognition algorithms proposed by Daugman [1] and Ma et al. [4,5] and compare our approach with those methods on the combined data set. Figure 20 exhibits the ROC curves of the proposed algorithms with the curve evolution approach based on game-theoretic fusion for the nonhomogeneous combined data set. ROC curves of the approaches demonstrated in [1,4,5] are also plotted for comparison, and it is observed from this figure that the

Table 3 Comparison of CRR, and EER

Algorithm	Correct recognition rate (%)				
	ICE	CASIA	UBIRIS	WVU	Combined
(a) Comparison of CRR					
Daugman [1]	98.13	95.19	97.28	83.14	93.43
Ma et al. [5]	95.79	95.54	95.45	78.33	92.56
Ma et al. [4]	95.64	94.90	95.78	77.24	91.23
Proposed	98.29	97.23	97.41	96.43	97.17
Algorithm	Equal error rate (EER) (%)				
	ICE	CASIA	UBIRIS	WVU	Combined
(b) Comparison of EER					
Daugman [1]	0.49	1.80	0.96	8.45	6.38
Ma et al. [5]	1.72	2.07	1.21	10.50	6.40
Ma et al. [4]	1.50	2.62	1.13	11.43	8.72
Proposed	0.38	0.74	0.50	1.79	0.86

proposed algorithm achieves higher GAR with a very low EER of 0.86% for the combined data set. It means that the proposed algorithm achieves higher discriminating capabilities than the approaches proposed in [1,4,5]. Moreover, the approaches proposed in [1,4,5] were not adjusted specifically for the nonideal situation. The proposed segmentation algorithm based on the noncooperative game-theoretic fusion obtains a higher GAR of 97.12% at the fixed FAR of 0.001% on the combined data set, which contains the iris images with the irregularities due to motion blur, off-angle gaze, diffusion, and other real-world problems. Therefore, the ROC curves in Fig. 20 reveal the effectiveness of the proposed scheme in a nonideal situation.

The major difficulty, which is common to any data set, is the segmentation error. The localization approach described in Sect. 3 works well for most of the cases even with the iris images of deviated gaze. The DLS-based elliptical fitting provides an initial estimate of the inner boundary, and the game-theoretic fusion approach localizes the iris and pupil regions accurately. In Table 3a and b, the proposed scheme exhibits the highest CRR for ICE, CASIA, WVU, and UBIRIS data sets. For the combined data set, we find the CRR of 97.17%, which reveals a top-class performance with respect to the nonideal data sets under consideration. The EER of the proposed approach on the combined data set is 0.86% and that is encouraging.

4.4 Discussions

Based on the above experimental results, we summarize the following salient points:

- To detect the inner and outer boundaries accurately, we apply a game-theoretic fusion strategy that shares the complementary strengths of the region-based segmentation and the gradient-based boundary-finding methods. Based on the segmentation results, we observe that the integrated segmentation approach is much more robust to the increasing noise and poor localization.
- The proposed segmentation scheme is also compared with the other state-of-the-art iris segmentation methods, and the results demonstrate that our algorithm performs better than the other approaches in the nonideal situations.
- A two-step image enhancement technique is applied where the first step enhances the quality of the iris image and the second step suppresses the effect of noise.
- We conduct our experimentation on four challenging iris data sets, and the experimental results exhibit an encouraging performance for the proposed iris recognition algorithm with respect to the recognition rates. We further apply the proposed scheme on the nonhomogeneous combined data set with a common set of parameters values and achieve reasonable performance.

5 Conclusions

The accurate segmentation of the iris plays an important role in iris recognition. The proposed iris segmentation algorithm achieves three performance goals. First, the game-theoretic integration algorithm brings together the region-based and boundary-based methods and operates different probability spaces into a common information-sharing framework. Second, the accurate localization of the iris regions from degraded eye images which are affected by severe gaze deviation, diffusion, non linear deformation, low intensity, poor acquisition process, eyelid and eyelash

occlusions and small opening of the eyes. Third, the proposed localization scheme based on game theory avoids the over-segmentation and performs well for blurred iris/sclera boundary. The image enhancement algorithm increases the quality of the iris image and reduces the effect of noise. We validate the proposed iris recognition scheme on the ICE 2005, the CASIA Version 3, the UBIRIS Version 1, WVU Nonideal, and also on the nonhomogeneous combined data sets with an encouraging performance. In future, we would like to extract the global textural and local topological features from the iris image and the corresponding match scores will be fused using the game-theoretic approach to improve the iris recognition performance further.

Acknowledgments This work was supported in part by NSERC Canada grant and by Concordia University research grant. Portions of this research work used ICE 2005 [52], CASIA Version 3 [53], UBIRIS Version 1 [54], and WVU [55] data sets.

References

1. Daugman, J.G.: High confidence visual recognition of persons by a test of statistical independence. IEEE Trans. Pattern Anal. Mach. Intell. **15**(11), 1148–1161 (1993)
2. Daugman, J.G.: How iris recognition works. IEEE Trans. Circuits Syst. Video Technol. **14**(1), 21–30 (2004)
3. Daugman, J.G.: The importance of being random: statistical principles of iris recognition. Pattern Recogn. **36**(2), 279–291 (2003)
4. Ma, L., Tan, T., Wang, Y., Zhang, D.: Personal identification based on iris texture analysis. IEEE Trans. Pattern Anal. Mach. Intell. **25**(12), 1519–1533 (2003)
5. Ma, L., Tan, T., Wang, Y., Zhang, D.: Efficient iris recognition by characterizing key local variations. IEEE Trans. Image Process **13**(6), 739–750 (2004)
6. Boles, W., Boashash, B.: A human identification technique using images of the iris and wavelet transform. IEEE Trans. Signal Process **46**(4), 1185–1188 (1998)
7. Wildes, R.P.: Iris recognition: an emerging biometric technology. Proc. IEEE **85**(9), 1348–1363 (1997)
8. Wildes, R., Asmuth, J., Green, G., Hsu, S., Kolczynski, R., Matey, J., McBride, S.: A machine-vision system for iris recognition. Mach. Vis. Appl. **9**, 1–8 (1996)
9. Schuckers, S.A.C., Schmid, N.A., Abhyankar, A., Dorairaj, V., Boyce, C.K., Hornak, L.A.: On techniques for angle compensation in nonideal iris recognition. IEEE Trans. Syst. Man Cybern. B **37**(5), 1176–1190 (2007)
10. Bowyer, K.W., Hollingsworth, K., Flynn, P.J.: Image understanding for iris biometrics: a survey. Comput. Vis. Image Underst. **110**(2), 281–307 (2008)
11. Daugman, J.G.: New methods in iris recognition. IEEE Trans. Syst. Man Cybern. B **37**(5), 1167–1175 (2007)
12. Vatsa, M., Singh, R., Noore, A.: Improving iris recognition performance using segmentation, quality enhancement, match score fusion, and indexing. IEEE Trans. Syst. Man Cybern. B **38**(4), 1021–1035 (2008)
13. Proenca, H., Alexandre, L.: Toward noncooperative iris recognition: a classification approach using multiple signatures. IEEE Trans. Pattern Anal. Mach. Intell. **29**(4), 607–612 (2007)
14. Zhang, D., Yu, L., Wang, K.: The relative distance of key point based iris recognition. Pattern Recogn. **40**(2), 423–430 (2007)
15. Ross, A., Shah, S.: Segmenting Non-ideal irises using geodesic active contours. In: Biometric Consortium Conference of IEEE Biometrics Symposium, pp. 1–6 (2006)
16. Shah, S., Ross, A.: iris segmentation using geodesic active contours. IEEE Trans. Info. Forensic Secur **4**(4) (2009)
17. Miyazawa, K., Ito, K., Aoki, T., Kobayashi, K., Nakajima, H.: An effective approach for iris recognition using phase-based image matching. IEEE Trans. Pattern Anal. Mach. Intell. **30**(10), 1741–1755 (2008)
18. Liu, X., Bowyer, K.W., Flynn, P.J.: Experiments with an improved iris segmentation algorithm. In: IEEE Workshop on Automatic Identification Advanced Technologies, pp. 118–123 (2005)
19. Liu, X., Bowyer, K.W., Flynn, P.J.: Experimental evaluation of iris recognition. IEEE Conf. Comput. Vis. Pattern Recogn. **3**, 158–165 (2005)
20. Hollingsworth, K.P., Bowyer, K.W.: The best bits in an iris code. IEEE Trans. Pattern Anal. Mach. Intell. **31**(6), 964–973 (2009)
21. Sudha, N., Puhan, N.B., Xia, H., Jiang, X.: Iris recognition on edge maps. IET Comput. Vis. **3**(1), 1–7 (2009)
22. Monro, D.M., Rakshit, S., Zhang, D.: DCT-based iris recognition. IEEE Trans. Pattern Anal. Mach. Intell. **29**(4), 586–595 (2007)
23. Kong, A.W.K., Zhang, D., Kamel, M.S.: An analysis of IrisCode. IEEE Trans. Info. Forensic Secur. **19**(2) (2010)
24. Sun, Z., Tan, T.: Ordinal measures for iris recognition. IEEE Trans. Pattern Anal. Mach. Intell. **31**(12), 586–595 (2009)
25. Roy K., Bhattacharya P.: Iris Recognition in nonideal situations. In: Information Security Conference, Springer Lecture Note Series in Computer Science, vol. 5735, pp. 143–150 (2009)
26. Roy, K., Bhattacharya, P.: Adaptive asymmetrical SVM and genetic algorithms based iris recognition. In: International Conference on Pattern Recognition, pp. 1–4 (2008)
27. Roy, K., Bhattacharya, P., Suen, C.Y.: Towards nonideal iris recognition based on level set method, genetic algorithms and adaptive asymmetrical SVMs. Int. J. Eng. Appl. Artif. Intell. Elsevier (2010, Accepted) doi:10.1016/j.engappai.2010.06.014
28. Kong, W., Zhang, D.: Accurate iris segmentation based on novel reflection and eyelash detection mode. In: IEEE International Symposium on Intelligent Multimedia, Video and Speech Processing, pp. 263–266 (2001)
29. Kong, W., Zhang, D.: Detecting eyelash and reflections for accurate iris segmentation. Int. J. Pattern Recogn. Artif. Intell. **17**(6), 1025–1034 (2003)
30. Zhou, Z., Du, Y., Belcher, C.: Transforming traditional iris recognition systems to work on non-ideal situations. IEEE Trans. Ind. Electr. **56**(8), 3203–3213 (2009)
31. He, Z., Tan, T., Sun, Z., Qiu, X.: Toward accurate and fast iris segmentation for iris biometrics. IEEE Trans. Pattern Anal. Mach. Intell. **31**(9), 1670–1684 (2009)
32. He, Z., Sun, Z., Tan, T., Qiu, X., Zhong, C., Dong, W.: Boosting ordinal features for accurate and fast iris recognition. In: Proceedings of IEEE Computer Society Workshop Biometrics at the Computer Vision Pattern Recognition Conference (2008)
33. Sung, H., Lim, J., Park, J., Lee, Y.: Iris recognition using collarette boundary localization. Int. Conf. Pattern Recogn. **4**, 857–860 (2004)
34. Son, B., Won, H., Kee, G., Lee, Y.: Discriminant iris feature and support vector machines for iris recognition. IEEE Int. Conf. Image Process **2**, 865–868 (2004)
35. Roy, K., Bhattacharya, P., Suen, Ching Y.: Recognition of unideal iris images using region-based active contour model and game theory. Int. Conf. Image Process, pp. 1705–1708 (2010)
36. Masek, L., Kovesi, P.: Biometric Identification Systems Based on iris Patterns. MATLAB source code, The school of Computer Science and Software Engineering, The University of Western Australia, Australia (2003)

37. Roy, K., Bhattacharya, P.: Optimal feature selection and classification for iris recognition. EURASIP J. Image Video Process. Article ID 743103, p. 20 (2008)
38. Roy, K., Bhattacharya, P.: Improvement of iris recognition performance using region-based active contour model, genetic algorithms and SVMs. Int. J. Pattern Recogn. Artif. Intell. (2010, Accepted)
39. Puhan, N.B., Sudha, N., Anirudh, S.K.: Efficient segmentation Technique for noisy frontal view iris images using Fourier spectral density. Signal Image Video Process (2010, to appear)
40. Chan, T.F., Vese, L.A.: Active contours without edges. IEEE Trans. Image Process. **10**(2), 266–277 (2001)
41. Malladi, R., Sethian, J.A., Vemuri, B.C.: Shape modeling with front propagation: a level set approach. IEEE Trans. Pattern Anal. Mach. Intell. **17**(2), 158–175 (1995)
42. Mumford, D., Shah, J.: Optimal approximation by piecewise smooth functions and associated variational problems. Commun. Pure Appl. Math. **42**(5), 577–685 (1989)
43. Sethian, J.A., Strain, J.: Crystal growth and dendritic solidication. J. Comput. Phys. **98**, 231–253 (1992)
44. Osher, S., Sethian, J.A.: Fronts propagating with curvature dependent speed: algorithms based on Hamilton–Jacobi Formulation. J. Comput. Phys. **79**, 12–49 (1988)
45. Chakraborty, A., Duncan, J.S.: Game-theoretic integration for image segmentation. IEEE Trans. Pattern Anal. Mach. Intell. **21**(1), 12–30 (1999)
46. Chakraborty, A., Staib, L.H., Duncan, J.S.: Deformable boundary finding in medical images by integrating gradient and region information. IEEE Trans. Pattern Anal. Mach. Intell. **15**(6), 859–870 (1996)
47. Fitzgibbon, A., Pilu, M., Fisher, R.B.: Direct least square fitting of ellipses. IEEE Trans. Pattern Anal. Mach. Intell. **21**, 476–480 (1999)
48. Gonzalez, R.C., Woods, R.E.: Digital image processing, 3rd edn. Prentice Hall, New Jersey (2007)
49. Jensen, A., La Cour-Harbo, A.: Ripples in Mathematics: The Discrete Wavelet Transform. Springer, Berlin (2001)
50. Mallat, S., Hwang, W.: Singularity detection and processing with wavelets. IEEE Trans. Inf. Theory **38**(2), 617–643 (1992)
51. Dutta, P.K.: Strategies and Games: Theory and Practice. MIT Press, Cambridge (1999)
52. Iris Challenge Evaluation (ICE) dataset found at http://iris.nist.gov/ICE/
53. CASIA-IrisV3, http://www.cbsr.ia.ac.cn/IrisDatabase.htm
54. UBIRIS dataset obtained from Dept. of Computer Sci., University of Beira Interior, Portugal. http://iris.di.ubi.pt/
55. Iris Dataset obtained from West Virginia University (WVU). http://www.citer.wvu.edu/biometric_dataset_collections